Journal of Membrane Science 428 (2013) 445–453

Contents lists available at SciVerse ScienceDirect

Journal of Membrane Science

journal homepage: www.elsevier.com/locate/memsci

Mixed matrix membranes containing MOFs for ethylene/ethane separation Part A: Membrane preparation and characterization

Jeroen Ploegmakers, Susilo Japip, Kitty Nijmeijer*

Membrane Science & Technology, MESA+ Institute for Nanotechnology, University of Twente, PO Box 217, Enschede 7500 AE, The Netherlands

ARTICLE INFO

Article history:
Received 19 September 2012
Received in revised form
30 October 2012
Accepted 2 November 2012
Available online 17 November 2012

Keywords:
Metal-organic frameworks
Gas separation
Ethylene
Mixed matrix membranes

ABSTRACT

Mixed matrix membranes (MMMs) containing three different metal organic frameworks (MOFs) (Cu_3BTC_2, FeBTC and MIL-53 (Al)) as filler in P84 were prepared and characterized in terms of ethylene/ethane separating ability. SEM, TGA and DSC suggest the absence of non-selective voids in the Cu_3BTC_2 and FeBTC MMMs. Gas permeation experiments confirmed this, and showed an increase in ethylene/ethane selectivity of 73% to a value of 7.1, while ethylene permeability remained constant at 17×10^{-18} mol m/(m^2 s Pa) with addition of 20 wt% Cu_3BTC_2. Addition of 20 wt% FeBTC showed a reduced permeability, caused by the formation of a denser intermediate layer, and no significant change in selectivity. Addition of MIL-53 led to increased permeabilities and no change in selectivity, which is probably the result of the formation of non-selective voids or the absence of inherent selectivity of MIL-53.

© 2012 Elsevier B.V. All rights reserved.

1. Introduction

Ethylene is the single largest produced chemical and used for the production of important products like low and high-density polyethylene, ethylene oxide, ethylene dichloride and ethylbenzene [1]. Due to their almost similar boiling points, both ethylene and ethane, culminate in the product stream after the cracking process of naphtha. Since ethane can only be used as feed for the steam-cracker, separation of these components is required. Currently, ethylene/ethane separation is carried out by cryogenic distillation at 248 K and 2.2 MPa, consuming large amounts of energy [2]. Yet significant energy reductions of 30% can be obtained by the use of hybrid membrane-distillation units [3]. However, the best performing membranes reported for the binary ethylene/ethane separation, are 6FDA-based polyimide membranes ($\alpha = 3.2$, $P = 0.85$ Barrer), but their performance is still too low to be economical viable [4]. Also, the permeability–selectivity tradeoff and the plasticizing nature of these high performing glassy polymers make them less suitable for industrial applications [5–7]. Since both permeability and selectivity need to be improved, much effort is put into overcoming this upper bound. Carbon membranes have shown to possess higher permeabilities and selectivities than their polymeric precursors [8–10]. However, they suffer from poor reproducibility due to marginal changes in the pyrolysis atmosphere and poor mechanical stability [11]. Another approach is facilitated transport membranes (FTMs) which have already been studied for over 30 years [12]. The transport mechanism relies on the reversible interaction between metal-ions and olefins, as described by the Dewar–Chatt–Duncanson model, in order to selectively enhance the olefin flux through the membrane [13,14]. Although by using this concept it is possible to obtain both high permeabilities and selectivities, these membranes suffer usually from carrier poisoning, reduction of the complexing agent or leaching and are often not mechanically stable at process conditions [15–18]. Additionally, many FTMs need the presence of significant amounts of water vapor in the feed stream to induce facilitated transport, which is usually not present in current olefin/paraffin streams [19–23].

In the last decade, Metal-organic frameworks (MOFs) have gathered much interest. MOFs are 1D, 2D or 3D porous structures consisting of a metal ion coordinated by tunable organic linkers. A comprehensive overview on the possible configurations and implications of MOFs has been given by James [24]. This wide variety of possible structures led to an exponential growth in the number of MOFs synthesized [25]. MOFs possess high sorption capacities and exhibit sorption selectivity between different gasses because of size exclusion and affinity effects, which makes them useful for industrial applications like hydrogen and carbon dioxide storage and adsorbers/desorbers [26–30]. These properties make them also interesting as membrane materials [31–33]. Still, MOF membranes, like other inorganic membranes, are expensive to produce and suffer from poor mechanical stability [34].

To overcome these disadvantages, we propose to incorporate MOFs in polymer membranes to create mixed matrix membranes (MMMs) for the separation of ethylene and ethane, thereby

* Corresponding author. Tel.: +31 53 489 4185; fax: +31 53 4894611.
E-mail address: d.c.nijmeijer@utwente.nl (K. Nijmeijer).

0376-7388/$ - see front matter © 2012 Elsevier B.V. All rights reserved.
http://dx.doi.org/10.1016/j.memsci.2012.11.014

combining the superior gas separation performance of MOFs with cheap and mechanical stable polymers [35–39]. Basu et al. obtained both an increase in carbon dioxide permeance and carbon dioxide/methane selectivity by combining the commercial MOFs Cu_3BTC_2, ZIF-8 and MIL-53 with Matrimid. The effects were less pronounced with addition of ZIF-8 (Zn) and MIL-53 (Al). Also changing to carbon dioxide/nitrogen separation showed less significant improvements [36]. Dai et al. did find a significant increase in carbon dioxide permeance and a 20% enhanced carbon dioxide/nitrogen selectivity when ZIF-8 was combined with Ultem as polymer matrix [40]. Although the absolute permeance and selectivity values did not surpass the Robeson upper bound because of the intrinsic low permeability of the Ultem material, their work did show that ZIF-8 selectively enhanced the carbon dioxide permeability and that the choice of polymer matrix can be crucial to see any effects. A similar study was performed by Zhang et al., where they mixed ZIF-8 with 6FDA-DAM polyimide for the separation of propylene and propane [41]. They found increased propylene permeabilities and increased propylene/propane selectivities when ZIF-8 was added to the polymer matrix, but did not observe sorption selectivity and saw a much lower diffusion selectivity than expected for the ZIF-8 MOFs, which was attributed to the usage of smaller sized crystals compared to other studies. Nevertheless, the main reason of the enhanced separation was due to increased molecular sieving effects. Since ethylene and ethane have smaller dimensions than their C_3 counterparts, it is not expected to see significant improvements by using ZIF-8 MMMs for ethylene/ethane separation. On the other hand, the MOF Cu_3BTC_2 is reported to exhibit solubility selectivity towards olefins over paraffins due to copper(II)–olefin interaction [42,43].

Considering this, especially the investigation of the effect of Cu_3BTC_2 in relation to other MOFs in MMMs on the separation of ethylene and ethane is relevant. Cu_3BTC_2 can increase the ethylene permeability by increasing the solubility and diffusion of ethylene. Furthermore, addition of Cu_3BTC_2 can increase the solubility and diffusion selectivity and therefore the permeability selectivity. For comparison, two other MOFs with different metal ions will be investigated as well. First, FeBTC, containing iron(III) ions will be used as a control. In a recent study, it was found that the iron(III) MOF, MIL-100, did not show any selectivity towards propylene over propane, which is expected since iron(III) has less d-electrons than copper(II) and makes bonding to an olefin energetically unfavorable [44]. Therefore, if any increase in permeability selectivity is found, it is expected that this is caused only by an increase in diffusion selectivity as opposed to Cu_3BTC_2. Second, the MOF MIL-53, containing aluminium(III) ions, will be used to create MMMs. Similar to FeBTC, no ethylene-MIL-53 interactions are expected, which means that if permeability selectivity is increased due to addition of MIL-53, this has to be attributed to molecular sieving effects increasing the diffusion selectivity. The commercially available polyimide P84 is chosen as polymer phase because of its low permeability towards gasses, diffusion driven selectivity and plasticization resistant properties [45,46]. The choice for P84 as polymer phase is important for several reasons: because of its low permeable properties, it enables to easily identify influences of MOFs on the permeability in MMMs. Secondly, P84's diffusion driven selectivity ensures that MOF induced solubility selectivity changes in MMMs are well observed. Lastly, P84 shows reduced plasticization effects on the permeability and selectivity and therefore allows changes in membrane properties to be assigned to effects caused by the introduction of MOFs dispersed in the polymer matrix such as non-selective voids or new intermediate phases [47,48].

This paper (Part A) will focus on the preparation and characterization of MMMs containing 20 wt% Cu_3BTC_2, FeBTC and MIL-53. Characterization will be performed by a multitude of techniques such as SEM, TGA, DSC and gas sorption. Finally the gas separation performance of the prepared MOF-polymer membranes will be evaluated in terms of ethylene/ethane separation performance. Not only mixed gas separation experiments will be performed but also both low and high pressure separation behavior of the membranes will be evaluated. As such the effect of the type of MOF and mixed gas pressure on membrane permeability and selectivity will be identified. Part B will describe a more detailed study on the effect of addition of various Cu_3BTC_2 loadings on the permeability, solubility and diffusivity coefficient.

2. Theory

2.1. Sorption

Sorption isotherms provide information on the gas sorption potential of the MOFs. When multiple molecules adsorb on a single site, which often happens in case of metals because of their multiple number of possible ligand sites, the Sips sorption model can be applied and is for a one component system described by Eq. 1 [49]:

$$C = \frac{C'_S \times (b_S \times p)^{1/n}}{1+(b_S \times p)^{1/n}} \quad (1)$$

where C'_S (kmol/g) is the Sips capacity constant (kmol/g), b_S is the Sips affinity constant (1/bar), p is the pressure (bar) and n (−) is the sorption intensity, which is the number of molecules adsorbing to a single site. Although Eq. 1 can be extended into a two component system, it must be stressed that even though single component Sips parameters can be accurately obtained from Eq. 1, multi-component sorption behavior cannot necessarily be predicted [50]. For this reason, only single gas experiments will be performed.

2.2. Gas permeation

Gas permeation through a dense membrane takes place according to the well-known solution–diffusion mechanism [51]:

$$P_i = S_i \times D_i \quad (2)$$

where the permeability coefficient P_i in Barrer (1 Barrer = 10^{-10} cm^3(STP)cm/(cm^2 s cmHg) = 3.34×10^{-16} mol m/(m^2 s Pa)) is the product of the solubility coefficient (S_i) (cm^3(STP)/(cm^3 bar)) and the diffusion coefficient (D_i) (cm^2/s) of component i. The selectivity of a gas pair is the ratio of their permeability coefficients:

$$\alpha_{ij} = \frac{P_i}{P_j} = \left(\frac{D_i}{D_j}\right) \times \left(\frac{S_i}{S_j}\right) \quad (3)$$

where D_i/D_j is the diffusion selectivity and S_i/S_j the solubility selectivity of components i and j, respectively. Diffusion coefficients increase with decreasing penetrant size, increasing polymeric fractional free volume, increasing polymer chain flexibility, increasing temperature and decreasing polymer–penetrant interactions [52]. On the other hand, solubility coefficients increase with increasing polymer–penetrant interactions, decreasing temperature and increasing condensability of the penetrant.

2.3. Mixed matrix membranes

The Maxwell model is often used to quantitatively describe the transport properties of gasses through MMMs. It assumes a uniform distribution of the dispersed phase and no formation of tertiary phases (e.g., non-selective voids or intermediate phases). The permeability of a gas through a MMM (P_{eff}) is given by:

$$P_{eff} = P_c \frac{P_d \times 2P_c \times 2\varphi_d(P_c - P_d)}{P_d \times 2P_c \times \varphi_d(P_c - P_d)} \quad (4)$$

where P_c and P_d are the permeabilities (10^{-16} mol m/(m^2 s Pa) of the continuous (polymer) and dispersed (MOF) phase, respectively, and φ_d is the volume fraction of the dispersed phase. Since it is often not possible to obtain the dispersed phase permeability data directly, the Maxwell model can be used to make accurate predictions by measuring MMMs with various amounts of dispersed phase.

Moore et al. have made a thorough categorization of the possible situations that can occur when particles are placed in a polymer matrix and divided these into six cases [48]. Case 0 is the ideal case in which there is perfect interaction between filler and matrix. The effective permeability will be described by the Maxwell model of Eq. 4. Case I–III are the result when stresses occur during the membrane formation process. Case I arises when a rigidified polymer layer is formed between the bulk polymer and the filler. This is usually accompanied by an increase in T_g or the presence of a second T_g at a higher temperature. Case II and III represent the 'sieve-in-a-cage' morphology in which non-selective voids are formed between the polymer and the filler, thereby enhancing the permeability while showing no change in selectivity. Case II can easily be observed by SEM images since the voids are usually large, while Case III shows much smaller nano sized voids. Case IV occurs when impermeable particles or strong sorbents are added to the polymer phase, which hinder the transport of the penetrant. This results in lower permeabilities with unchanged selectivities. Finally, Case V describes the situation, much like Case I, in which there is a layer of reduced permeability around the fillers.

3. Experimental

3.1. Materials

Lenzing P84 polyimide (325 mesh, STD) was supplied by HP Polymer GmbH, Austria. *N*-methyl-2-pyrrolidone (NMP, 99% extra pure) was supplied by Acros Organics, Belgium. The MOFs copper benzene-1,3,5-tricarboxylate (Cu_3BTC_2), iron benzene-1,3,5-tricarboxylate (FeBTC) and aluminum terephthalate (MIL-53) were obtained from Sigma-Aldrich as Basolite C300, Basolite F300 and Basolite A100, respectively. The binary gas mixture ethylene/ethane ($80/20 \pm 0.4$ v/v%) was supplied by Praxair, the Netherlands. All chemicals were used without further purification.

3.2. Membrane preparation

3.2.1. Native P84 membranes

P84 polyimide powder was dried in a Heraus Instruments Vacutherm vacuum oven at 100 °C overnight before use. The P84 solution was prepared by mixing 15% (w/wt%) P84 in NMP as solvent. The solution was stirred at room temperature overnight. Afterwards, the P84 solution was filtered through a 15 μm metal filter and degassed using an ultrasound bath for at least 30 min. The filtered and degassed solution was cast on a glass plate by using a 0.47 mm casting knife. The cast membranes were dried at room temperature under nitrogen flow for at least 3 days before they were dried in a WTC Binder oven at 150 °C with nitrogen flow for 24 h. Finally, the dried membranes were peeled off from the glass plate and dried in the oven at 60 °C under nitrogen flow for at least 3 days.

3.2.2. Mixed matrix membranes

The MMM casting suspension was prepared by mixing as received MOFs (Cu_3BTC_2, FeBTC or MIL-53) in NMP as solvent. The suspension was stirred for 1 h and then sonicated using a Branson 5210 ultrasound bath (40 kHz) for 15 min. 10% of the total added amount of dried P84 powder was added to the MOF/NMP suspension and stirred until completely dissolved. Next, the remaining 90% of P84 powder was added and the mixture was stirred at least overnight. The weight ratio of P84/MOF was kept at 80/20 w/w%. The suspension was degassed using an ultrasound bath for at least 30 min and subsequently cast on a glass plate in a nitrogen box using a 0.47 mm casting knife. The cast membranes were dried at room temperature under nitrogen flow for at least 2 days. The membranes were then transferred into a WTC Binder oven at 150 °C under nitrogen flow for 24 h for further drying. The dried membranes were peeled off from the glass plate and dried in the oven at 60 °C under nitrogen flow for at least 3 days.

MMMs with 20% Cu_3BTC_2, 20% FeBTC and 20% MIL-53 in P84, (w/wt%) were prepared this way and used for further experiments.

All prepared membrane samples were cut into circles (ø 47 mm). The thickness of the samples was determined using an IP65 Coolant Proof digital Micrometer from Mitutoyo and found to be 46 ± 1 μm for the native P84 membranes, 66 ± 3 μm for Cu_3BTC_2 and FeBTC MMMs and 87 ± 2 μm for the MIL-53 MMMs.

3.3. SEM

Samples for scanning electron microscopy (SEM) were prepared by freezing the prepared membranes in liquid nitrogen and then breaking them to investigate homogeneity of the MOFs throughout the MMMs and compatibility between the MOFs and the polymer phase. The samples were dried in a vacuum oven at 30 °C overnight and coated with a thin gold layer using a Balzers Union SCD040 sputtering device under argon flow. Images of the cross-sectional membrane area were taken using a JEOL JSM-5600LV Scanning Electron Microscope and Semaphore software.

3.4. XRD

To determine the crystallinity of the obtained MOFs, X-Ray diffraction (XRD) of Cu_3BTC_2, FeBTC and MIL-53 was performed on a Bruker D2 PHASER. Scans were made from 5–50° 2θ with a step-size of 0.0202° in 42 min.

3.5. TGA

Investigation of the thermal stability of the MOFs, P84 and MMMs was performed by thermogravimetrical analysis (TGA) on a Perkin Elmer TGA 4000. At least 5 mg of each sample was placed into a small aluminum sample holder. Under a constant nitrogen flow of 20 mL per minute, the sample was heated up to 900 °C at a heating rate of 20 °C per minute after initially being held at 30 °C for 1 min.

3.6. DSC

Differential scanning calorimetry (DSC) was performed on a Perkin Elmer DSC 8000 in order to determine the glass transition temperature (T_g) of P84 and the MMMs. At least 2 mg of each sample was placed into an aluminum sample holder. The sample was held at 30 °C for 1 min before being heated. The P84 membrane was heated to 400 °C, while the MMMs were heated till 350 °C at a constant heating rate of 100 °C per minute. Afterwards, the sample was held for 1 min at the maximum temperature and then cooled down to 30 °C at a cooling rate of 100 °C per minute. This cycle was repeated three times, and data from the last heating scan were used to determine the (T_g), which is defined as the midpoint of the heat capacity transition.

3.7. Gas sorption

A magnetic suspension balance (MSB) (Rubotherm) was used to perform sorption measurements. Sorption measurements are used to construct sorption isotherms in order to determine capacity and affinity constants for various MOFs according to Eq. 1. The mass uptake of the sample (m_t) was calculated according to Eq. 5:

$$m_t = w_t - \left(w_0 - V_t \times \rho_{gas}\right) \quad (5)$$

where w_0 is the weight of the sample (g) at zero sorption, V_t is the volume (cm^3 of the sample at time t (s) and ρ_{gas} is the density of the gas (g/cm^3). The recorded weight (w_t (g)) was corrected for buoyancy according to the Archimedes principle.

Pure gas sorption of ethylene and ethane was determined in all samples. The concentration of gas in the sample was calculated from the mass uptake, the volume of the sample (calculated from the density of the sample as determined using a Micromeritics AccuPyc 1330 pycnometer at 26.0 ± 0.8 °C), the molar volume and the molecular weight of the gas. The molar volume of the gas was calculated using the Peng–Robinson equation of state.

A minimum of 50 mg was used as sample. Before each sorption run, the sample was degassed at 35 °C. A sorption run consisted of a stepwise increase in pressure until equilibrium was reached. A pseudo-equilibrium was taken if no equilibrium was reached in 24 h. All measurements were performed at a constant temperature of 35 ± 0.5 °C. Sorption isotherms were curve fitted using Eq. 1 for all MOF particles to investigate the potential ethylene and ethane sorption capacity.

3.8. Gas permeation

Gas permeation experiments were performed on native P84 membranes and all MMMs. Permeability measurements were performed by using the constant volume, variable pressure method with vacuum at the permeate side as described elsewhere [53]. Partial pressures higher than 1 bar were replaced by their corresponding fugacities to correct for non-ideal behavior.

Alternating single gas nitrogen and ethylene/ethane mixed gas permeation measurements were performed on the same membrane samples. The nitrogen feed pressure was kept constant at 5 bar to investigate plasticization effects. The ethylene/ethane feed pressure was increased from 5 bar, to 10 bar and eventually to 15 bar.

In the case of a mixed gas feed, both feed and permeate were analyzed by a Varian 3900GC gas chromatograph using an Alltech Alumina F-1 60/80 packed bed column at 150 °C. Enough permeate was collected to achieve a signal/noise (S/N) ratio of at least 10. Mixed gas selectivity was calculated according to Eq. 6:

$$\alpha_{ij} = \frac{y_i/y_j}{x_i/x_j} \quad (6)$$

where y_j and x_j are the downstream and upstream mole fractions of compound j, respectively.

3.9. Analysis of variance

Analysis of variance (ANOVA) was used in order to determine if the addition of MOFs to the polymer matrix had a significant effect on the permeability and selectivity of ethane and ethylene. ANOVA is a powerful statistical method to determine the effect of a controlled source of variation in comparison to the random variation in the obtained results that always occurs in experiments. ANOVA also shows if deviations from the mean are statistically significant. The F value, which is the ratio of the within-sample mean square and the between sample mean square ($F > 1$), is compared to the critical F value (F_{crit}) for the appropriate number of degrees of freedom and a confidence interval of 95%. The null hypothesis is rejected if $F > F_{crit}$. The null hypothesis is defined as the means of the samples do not differ significantly.

4. Results and discussion

4.1. MOF characterization

4.1.1. General properties

The characteristics of the MOFs used in this work are shown in Table 1. Cu_3BTC_2 has the highest BET surface area, followed by FeBTC and MIL-53, which has the lowest. The average particle size of Cu_3BTC_2 is 15.96 μm, which is approximately half that of MIL-53. No particle size information was provided on FeBTC. Within the experimental error, all MOFs show similar densities of ~ 1.7 g/cm^3.

The densities of the MOFs are higher than those typical for polymer solutions, which means that during the casting procedure, MOF particles might sediment to the bottom. The densities obtained with pycnometry show large discrepancies with values provided by the manufacturer, caused by a different measurement technique of the manufacturer that does not account for the porosity of the materials. The high D50 value of 31.55 μm for MIL-53 might pose a problem for membrane fabrication since large particles require thick films to be completely encapsulated and reduce defects. The high BET surface area for Cu_3BTC_2 makes these particles promising for ethylene adsorption, which in turn can enhance the gas separation performance in MMMs.

4.1.2. SEM

Fig. 1 shows SEM images of Cu_3BTC_2, FeBTC and MIL-53, respectively. Cu_3BTC_2 shows particles with a crystalline structure and a diameter between 1 and 15 μm, which is slightly lower than the D50 value reported in Table 1. The particle diameter of FeBTC varies between 3 and 30 μm. MIL-53 shows large 80 μm crystalline particles, which can be expected based on Table 1. The large MIL-53 particles can pose a problem during the membrane formation since they are larger than the thickness of typical symmetric dense flat sheet membranes, which can lead to membrane defects. To avoid these problems, the MIL-53 particles were grinded to obtain sub 30 μm particles. No clear crystalline structure can be observed for FeBTC like is the case for Cu_3BTC_2.

4.1.3. XRD

XRD measurements were performed to gain further insight on the crystallinity of the MOF particles. Fig. 2 shows the XRD spectra of Cu_3BTC_2, FeBTC and MIL-53. Both Cu_3BTC_2 and MIL-53 have a crystalline structure which is in accordance with literature [55]. FeBTC on the other hand, shows an amorphous structure due to the absence of peaks caused by scattering of the X-Rays. To the best of the author's knowledge, there are no reports in literature about the effect of the MOF crystallinity in MMMs on gas permeation.

Table 1
Properties of Cu_3BTC_2, FeBTC and MIL-53.

	BET surf. area (m^2/g) [54]	Particle size (D50) (μm) [54]	Density* (g/cm^3)
Cu_3BTC_2	1500–2100	15.96	1.663
FeBTC	1300–1600	–	1.677
MIL-53	1100–1500	31.55	1.642

* Experimentally determined with Micromeritics AccuPyc 1330 pycnometer.

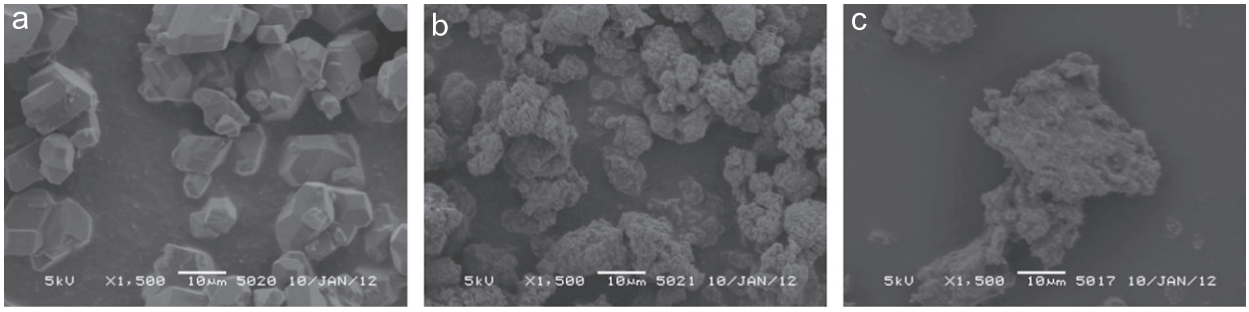

Fig. 1. SEM images of (a) Cu_3BTC_2, (b) FeBTC and (c) MIL-53, respectively.

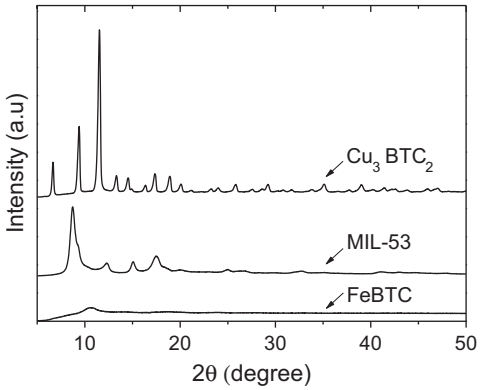

Fig. 2. XRD of Cu_3BTC_2, FeBTC and MIL-53.

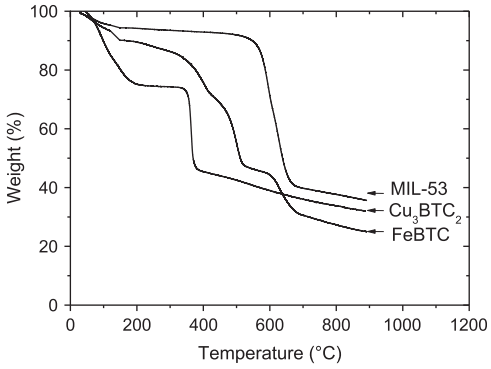

Fig. 3. TGA of Cu_3BTC_2, FeBTC and MIL-53 MOFs.

4.1.4. TGA

The thermal stability of all MOFs was investigated by means of TGA and is shown in Fig. 3. Cu_3BTC_2 shows a weight loss of 26% up to 200 °C, which indicates a loss of hydrated water [55]. When the temperature is increased from 310 °C to 375 °C, Cu_3BTC_2 loses another 27% of its initial weight and this marks the start of the degradation process that continues up to the final temperature of 900 °C where only 32% of its initial weight is remained.

A weight loss of 10% is observed for FeBTC up to 200 °C. This can be attributed to a lower amount of hydrated water compared to Cu_3BTC_2. From this temperature upwards till the final temperature of 900 °C, the weight decreases continuously with increasing temperature. This weight decrease is caused by the degradation of FeBTC into gaseous products [56]. The largest weight loss is observed between 400 and 500 °C with a weight loss of 27%.

In contrast to Cu_3BTC_2 and FeBTC, MIL-53 only shows a 5% weight loss when heated to 200 °C. This can be attributed to a low amount of hydrated water and is consistent with literature which reports a low adsorption of water molecules per MOF molecule (<2) [57]. When the temperature is increased to 550 °C, an additional weight loss of only 3% is visible. This indicates that, up to this temperature, MIL-53 forms almost no gaseous products as a consequence of degradation. A large weight decrease of 40% is observed when the sample is further heated to 700 °C, indicating that in this temperature range, MIL-53 decomposes into gaseous products.

Given the above, we conclude that Cu_3BTC_2, FeBTC and MIL-53 are thermally stable up to 200, 350 and 550 °C, respectively. This is relevant for the preparation of MMMs, since heating the polymer matrix above the T_g or T_m can reduce the formation of non-selective voids [48].

4.1.5. Static gas sorption

The sorption capacity of polymer membranes can be increased by incorporating MOFs with a higher sorption capacity into the polymer phase. Therefore, the sorption behavior of ethylene and ethane in Cu_3BTC_2, FeBTC and MIL-53 was investigated and the obtained data were fitted using Eq. 1. The resulting sorption isotherms and the ideal solubility of the MOFs as function of the feed fugacity are shown in Fig. 4a and b, respectively.

Fig. 4a shows a significant difference in sorption behavior between Cu_3BTC_2 on one hand and FeBTC and MIL-53 on the other. Cu_3BTC_2 has the highest ethylene sorption with a sorption capacity of around 390 cm^3(STP)/cm^3 at 11 bar, which is comparable to values found in literature for carbon dioxide, while FeBTC and MIL-53 have a sorption capacity of only 170 and 150 cm^3(STP)/cm^3, respectively, at 11 bar [58]. In order to understand the origin of these differences, the sorption data were fitted using Eq. 1 and the obtained parameters are shown in Table 2. The maximum Sips sorption capacity, C'_S, of Cu_3BTC_2 is twice as high compared to that of FeBTC and MIL-53. The Sips affinity parameter b_S for both ethylene and ethane in Cu_3BTC_2 is roughly 4–8 times higher compared to that of FeBTC and MIL-53. As shown in Table 1, the BET surface area of Cu_3BTC_2 is larger in comparison to that of FeBTC and MIL-53. Given these three properties, ethylene and ethane sorption is significantly higher in Cu_3BTC_2 as compared to FeBTC and MIL-53, since there is more surface area available in Cu_3BTC_2 and there are stronger interactions between the gas molecules and the copper(II) ions. In addition, multiple ethylene molecules can adsorb per sorption site as represented by $n>1$.

Fig. 4b shows that Cu_3BTC_2 has the highest ideal sorption selectivity with a maximum of 1.5 at 0.5 bar compared to FeBTC and MIL-53 with an ideal sorption selectivity of 1.0 for both MOFs. The presence of an ideal ethylene/ethane sorption selectivity in Cu_3BTC_2 can be unexpected at first because the reversible bonds formed between the metal ion and the olefin are based on the donation of d-electrons from the metal ion to the empty π^*-antibonding orbital as explained by the Dewar–Chatt–Duncanson model. Since the copper(II) ions in Cu_3BTC_2 only have 9 d-electrons, the interaction between the nucleus of the copper(II) ions and the surrounding electrons is much stronger and donation of d-electrons

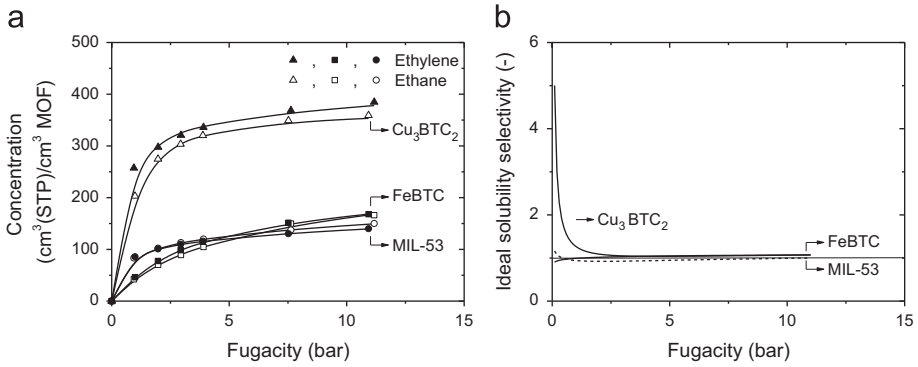

Fig. 4. (a) Sorption isotherms of ethylene (▲,■,●) and ethane (△,□,○) in Cu_3BTC_2 (triangle), FeBTC (square) and MIL-53 (circle) as function of fugacity. Lines indicate isotherms fitted using the Sips model and (b) Ideal solubility selectivity of Cu_3BTC_2, FeBTC and MIL-53 as function of fugacity.

Table 2
Fit results of the sorption isotherms of ethylene and ethane using the Sips model for various MOFs.

	Cu_3BTC_2			FeBTC			MIL-53		
	C'_S	b_S	n	C'_S	b_S	n	C'_S	b_S	n
Ethylene	513	1.07	2.25	263	0.17	1.09	278	0.13	2.48
Ethane	377	1.16	0.85	223	0.27	0.97	247	0.18	2.70

requires much more energy. Yet olefin/paraffin selectivity in Cu_3BTC_2 has been observed by other researchers as well and can be caused by the fact that 25% of the copper(II) ions–olefin bond strength is caused by π-donation of electrons from the olefin π-orbital to the copper(II) ions-orbital [42,59]. So although the copper(II) ions-olefin complexation is much weaker as compared to the copper(I) ions–olefin complexation, there is still some interaction which causes sorption selectivity between olefins and paraffins and this can be utilized to increase the ethylene/ethane selectivity in MMMs. The absence of any ideal sorption selectivity in the case of FeBTC and MIL-53 indicates that if any increase in selectivity is found during gas permeation experiments, this increase is caused by an increase in diffusion selectivity as the result of molecular sieving effects.

4.2. Membrane characterization

4.2.1. SEM

Fig. 5a–c show the cross-sectional SEM images of the 20 wt% Cu_3BTC_2, FeBTC and MIL-53 MMMs, respectively. The 20 wt% Cu_3BTC_2 and FeBTC MMMs show a good adhesion between the P84 and MOFs, in contrast to the 20 wt% MIL-53 MMM, shown in Fig. 5c, which shows small voids spread across the MIL-53-P84 layer. This might be caused by smaller MIL-53 crystals being removed from the polymer matrix during sample preparation for SEM. Another reason could be that there is an incompatibility between the polymer matrix and the MIL-53 particles, creating large non-selective voids.

Apart from the 20 wt% MIL-53 MMM, the avoidance of larger non-selective voids in the MMMs has been accomplished by choosing an appropriate polymer as the matrix in combination with a suitable membrane fabrication process [48]. The combination of polar Cu_3BTC_2 and FeBTC MOFs inside a polar P84 membrane allows for polar interactions, thereby improving the polymer–MOF adhesion. Also, the gradual addition of the P84 powder to the MOFs during the membrane fabrication process prevents agglomeration of both the MOF particles and the P84 polymer. Unfortunately, all MMMs showed an asymmetric structure consisting of a P84 and a MMM layer. This is caused by the slow evaporation of NMP, which allows the MOF particles to descend to the glass side of the membrane. Although a more homogenous distribution was initially preferred instead of this asymmetric morphology, it was found that the inhomogeneity had no negative impact on the adhesion between the polymer and the MOF particles and consequently, on the permeability, as will be discussed later.

4.2.2. TGA

Fig. 6 shows the TGA of native P84 and the P84 MMMs with 20 wt% Cu_3BTC_2, FeBTC and MIL-53. The native P84 membrane has a weight loss of only 1.2% when the temperature is increased to 175 °C. This is caused by evaporation of adsorbed solvent. An additional 9.5% of the weight is lost when the temperature is increased to 400 °C, which marks the start of the degradation process. At the final temperature of 900 °C, P84 has lost 46% of its original weight.

All MMMs show a thermal stability which is a linear contribution of native P84 and the pure MOFs shown in Fig. 3; besides the decomposition stages of native P84, an additional decomposition stage appears, which coincides with the decomposition of the pure MOFs. The 20 wt% Cu_3BTC_2 MMM shows a weight loss of 3.2% when the temperature is increased to 175 °C, which is attributed to the large amount of hydrated water in Cu_3BTC_2. The 20 wt% MIL-53 MMM has also similar decomposition stages as the native P84 membrane. Only the second decomposition stage at 600 °C shows a higher weight loss of 41% compared to 35% for the native P84 membrane. This is due to the additional decomposition of MIL-53, which happens at this temperature as can be seen in Fig. 3. Up to 400 °C, the 20 wt% FeBTC MMM shows similar weight loss compared to the native P84 membrane. When the temperature is further increased, the weight loss of the FeBTC MMM starts to increase and deviate from P84 due to degradation of the FeBTC MOF as shown in Fig. 3. The degradation of the FeBTC MMM continues till the final temperature of 900 °C when 65% of its initial weight is lost.

The TGA results presented in Fig. 6 indicate thermally stable P84 membranes and 20 wt% Cu_3BTC_2 and MIL-53 MMMs, up to 350 °C. From this temperature onwards, Cu_3BTC_2 starts to decompose. TGA of the pure MOFs, as shown in Fig. 3, already showed decomposition of FeBTC above 200 °C, which means the 20 wt% FeBTC MMM cannot be heated above this temperature without degradation. These results indicate that if the T_g of P84 is equal or higher than 200 or 350 °C, at which degradation of the MOFs occurs, it will not be possible to erase the sample history of the 20 wt% FeBTC or Cu_3BTC_2 and MIL-53 MMM, respectively. For this reason and to investigate polymer-MOF interactions, DSC measurements are performed, which will be discusses in the next paragraph.

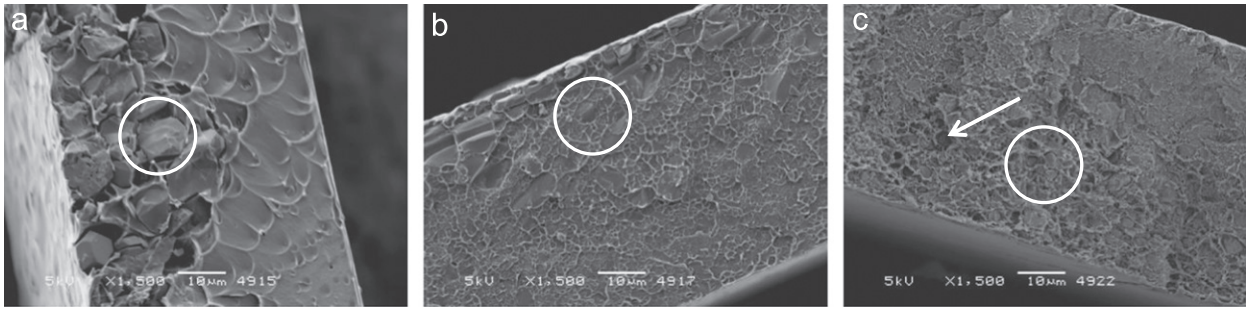

Fig. 5. SEM images of P84 MMMs with (a) 20 wt% Cu_3BTC_2 (b) 20 wt% FeBTC and (c) 20 wt% MIL-53. Particles are indicated by a white circle. An example of a void is indicated by a white arrow.

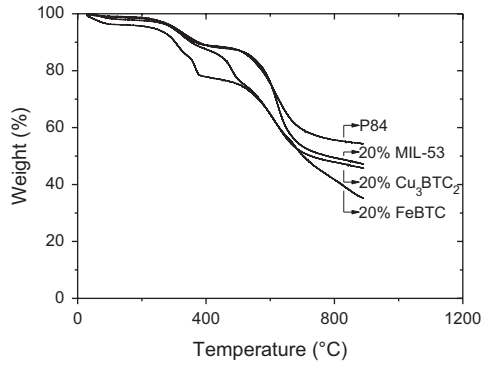

Fig. 6. TGA of P84 MMMs with 20 wt% Cu_3BTC_2, FeBTC and MIL-53.

Table 3
T_g of native P84 and P84 MMMs with various types of MOFs.

Polymer	MOF type added	MOF loading (wt%)	T_g (°C)
P84	–	0	345
P84	Cu_3BTC_2	20	329
P84	MIL-53	20	344
P84	FeBTC	20	–

4.2.3. DSC

DSC analysis was performed on native P84 and all MMMs to determine the glass transition temperature and to investigate changes in chain flexibility when MOFs are added to the polymer matrix. As shown in Table 3, the T_g of P84 is located at 345 °C. When 20 wt% Cu_3BTC_2 is added to the polymer matrix, a decrease in T_g of 16 °C to 329 °C is visible. This decrease in T_g is caused by disruption of physical crosslinks between the polymer chains due to the introduction of Cu_3BTC_2 crystals, which results in the formation of a more flexible intermediate phase between the polymer and the MOF.

The P84 MMM with 20 wt% MIL-53 has a T_g of 344 °C, which is only 1 °C lower than the T_g of P84. This reveals that there is neither disruption of polymer chain packing, nor formation of any intermediate phase and can imply that non-selective voids have been formed during the membrane fabrication process. It was not possible to determine the T_g of the 20 wt% FeBTC MMM because of the decomposition of FeBTC that takes place from 200 °C and onwards which is far below the T_g of P84.

Since the T_g of P84 and the P84 MMMs is equal to their corresponding decomposition temperatures as shown in Fig. 6, it is not possible to anneal the membranes and erase their history. In order to obtain comparable results, all membranes were fabricated such that all samples had the same history. Differences in sample history can affect permeabilities and selectivities as the result of physical aging [60].

4.2.4. Gas permeation measurements

To investigate the effect of various MOFs (i.e., Cu_3BTC_2, FeBTC and MIL-53) in MMMs on the ethylene permeability and ethylene/ethane selectivity, gas permeation experiments at 5, 10 and 15 bar total pressure were performed. Results are summarized in Fig. 7.

Fig. 7a shows the mixed gas ethylene permeability for native P84 and 20 wt% Cu_3BTC_2, FeBTC and MIL-53 MMMs at feed pressures ranging from 5 to 15 bar. At 5 bar mixed gas feed pressure, the permeability of the 20 wt% Cu_3BTC_2 MMM does not increase significantly compared to the permeability native P84 which is found to be 17×10^{-18} mol m/(m^2 s Pa). This indicates that there are no non-selective voids present in the MMMs as these would increase the permeability. Also, Fig. 7a shows that there is a reduction in permeability visible to 10×10^{-18} mol m/(m^2 s Pa) for the 20 wt% FeBTC MMM as compared to the native P84 membranes. A reduction in permeability with the introduction of particles to polymer membranes has also been observed by other researchers [47,61] and was well described by Moore et al. [48] where this phenomenon is classified as Case I or Case V. On the other hand, there is a significant increase in permeability for the 20 wt% MIL-53 MMM to 32×10^{-18} mol m/(m^2 s Pa). There are two possibilities to explain this result. First, the addition of MIL-53 could introduce non-selective voids or Case II behavior. Since it was already shown in Fig. 3 that MIL-53 adsorbs the least amount of water out of the MOFs investigated, this indicated that MIL-53 was less polar than Cu_3BTC_2 and FeBTC and therefore could have a reduced interaction with the polar P84 polymer. Also, some minor voids were observed in the SEM image shown in Fig. 5c. The second reason could be that both ethylene and ethane diffuse through MIL-53 without any interactions, in contrast to Cu_3BTC_2. This allows for a higher permeability for the penetrants in the MMM containing MIL-53 and this is also supported by the fact that the sorption capacity for both ethylene and ethane and the Sips affinity constant in MIL-53 are low as was shown in Table 2. An increase in permeability without increase in selectivity has also been reported for O_2/N_2 separations using MOF MMMs [62].

When the effect of feed pressure on the ethylene permeability of the different MOF containing MMMs is investigated, it can be seen that the permeability decreases in all cases with increasing feed pressure up to 15 bar. This is consistent with the dual-mode behavior in glassy polymers [63,64]. In addition, no signs of induced plasticization were observed within the pressure range studied.

Fig. 7b shows the mixed gas ethylene/ethane selectivity for native P84 and 20 wt% Cu_3BTC_2, FeBTC and MIL-53 MMMs at a feed pressure ranging from 5 to 15 bar. At 5 bar mixed gas feed

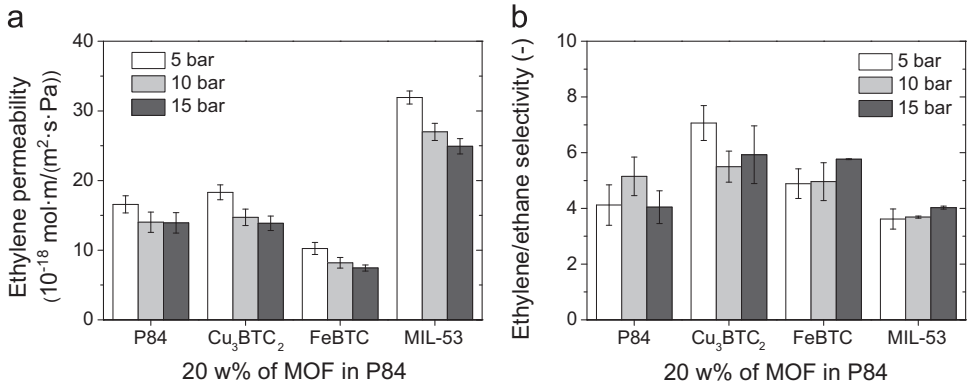

Fig. 7. Average ethylene permeability (a) and ethylene/ethane selectivity (b) ($\pm 2\sigma$) of native P84 and 20 wt% Cu_3BTC_2, FeBTC and MIL-53 MMMs at 5, 10 and 15 bar mixed gas feed pressure.

pressure, the ethylene/ethane selectivity is almost doubled from 4.1 to 7.1 when 20 wt% Cu_3BTC_2 is added to the polymer matrix. The selectivity does not significantly increase at 5 bar feed pressure when 20 wt% FeBTC or MIL-53 is added to the polymer matrix. This is consistent with the sorption data reported in Fig. 4b, which showed that only Cu_3BTC_2 provided ethylene/ethane sorption selectivity higher than 1.0. Combined with the permeability data shown in Fig. 7a, addition of FeBTC to the P84 matrix shows either Case I or Case IV behavior. Since it was not possible to determine the T_g of these membranes, it is impossible to discriminate between the two. In any case, addition of FeBTC particles does provide neither any additional solubility nor diffusion selectivity. The fact that MIL-53 does not provide an increase in selectivity indicates that there are non-selective voids present or that there is no selective reversible interaction between the aluminium(III) ion and the ethylene double bond. This lack of interaction is expected since aluminium(III) neither has the necessary d-electrons to donate to ethylene, nor the empty s-orbital required to accept electrons from the ethylene π-orbitals. However it also shows that MIL-53 does not provide any additional diffusion selectivity. Therefore, MMMs containing MIL-53 can either be the result of Case 0 where MIL-53 has no additional selectivity, or the result of Case II in which non-selective voids are responsible for the increase in permeability.

5. Conclusions

Native P84 membranes and MMMs with 20 wt% Cu_3BTC_2, FeBTC and MIL-53 have been successfully prepared. Ethylene/ethane selectivity increased up to 73% from 4.1 to 7.1 when 20 wt% Cu_3BTC_2 was added to the P84 matrix, while the permeability remained constant at 17×10^{-18} mol m/(m^2 s Pa), which confirms, in combination with DSC data, the absence of non-selective voids in the MMMs. Addition of FeBTC MOFs resulted in reduced permeabilities of 10×10^{-18} mol m/(m^2 s Pa) at 5 bar feed pressure with no significant increase in selectivity, indicating the formation of a denser intermediate phase. When MIL-53 MOFs were added to the polymer phase, the permeability increased to 32×10^{-18} mol m/(m^2 s Pa), while the selectivity remained constant, indicating either the formation of non-selective voids, or the non-selective ethylene/ethane properties of MIL-53 as was shown with static sorption experiments. Increasing the feed pressure from 5 to 15 bar resulted in slightly reduced permeabilities for all membranes, which is typical dual-mode behavior in glassy polymers. In addition, plasticization was not observed within the pressure range studied.

Acknowledgments

This project is financially supported by AgentschapNL. The authors would like to thank ECN, Dow and SolSep for the fruitful discussions and Dr. H.H.J.L. Ploegmakers for his help regarding the statistical analysis.

References

[1] 232nd ACS national meeting, San Francisco, Sept. 10–14, Chemical and Engineering News 84 (2006) 59–236.
[2] Z. Wu, S.S. Han, S.H. Cho, J.N. Kim, K.T. Chue, R.T. Yang, Modification of resin-type adsorbents for ethane/ethylene separation, Ind. Eng. Chem. Res. 36 (1997) 2749–2756.
[3] J.A. Caballero, I.E. Grossmann, M. Keyvani, E.S. Lenz, Design of hybrid distillation-vapor membrane separation systems, Ind. Eng. Chem. Res. 48 (2009) 9151–9162.
[4] C. Staudt-Bickel, W.J. Koros, Olefin/paraffin gas separations with 6FDA-based polyimide membranes, J. Membr. Sci. 170 (2000) 205–214.
[5] L.M. Robeson, Correlation of separation factor versus permeability for polymeric membranes, J. Membr. Sci. 62 (1991) 165–185.
[6] L.M. Robeson, The upper bound revisited, J. Membr. Sci. 320 (2008) 390–400.
[7] C. Staudt-Bickel, W.J. Koros, Improvement of CO_2/CH_4 separation characteristics of polyimides by chemical crosslinking, J. Membr. Sci. 155 (1999) 145–154.
[8] J.I. Hayashi, H. Mizuta, M. Yamamoto, K. Kusakabe, S. Morooka, S.H. Suh, Separation of ethane/ethylene and propane/propylene systems with a carbonized BPDA-pp'ODA polyimide membrane, Ind. Eng. Chem. Res. 35 (1996) 4176–4181.
[9] M. Yoshino, S. Nakamura, H. Kita, K.I. Okamoto, N. Tanihara, Y. Kusuki, Olefin/paraffin separation performance of carbonized membranes derived from an asymmetric hollow fiber membrane of 6FDA/BPDA-DDBT copolyimide, J. Membr. Sci. 215 (2003) 169–183.
[10] L. Xu, M. Rungta, W.J. Koros, Matrimid® derived carbon molecular sieve hollow fiber membranes for ethylene/ethane separation, J. Membr. Sci. 380 (2011) 138–147.
[11] M. Kiyono, P.J. Williams, W.J. Koros, Effect of pyrolysis atmosphere on separation performance of carbon molecular sieve membranes, J. Membr. Sci. 359 (2010) 2–10.
[12] O.H. LeBlanc Jr, W.J. Ward, S.L. Matson, S.G. Kimura, Facilitated transport in ion-exchange membranes, J. Membr. Sci. 6 (1980) 339–343.
[13] M.J.S. Dewar, A review of the pi-complex theory, Bull. Soc. Chim. 18 (1951) 8.
[14] J. Chatt, L.A. Duncanson, Olefin co-ordination compounds. Part III. Infra-red spectra and structure: attempted preparation of acetylene complexes, J. Chem. Soc. (Resumed) (1953) 2939–2947.
[15] S.B. Hamouda, Q.T. Nguyen, D. Langevin, S. Roudesli, Facilitated transport of ethylene in poly (amide 12-block tetramethylenoxide) copolymer/$AgBF_4$ membranes containing silver (I) and copper (I) ions as carriers, J. Appl. Sci. 8 (2008) 1310–1314.
[16] M. Teramoto, H. Matsuyama, T. Yamashiro, Y. Katayama, Separation of ethylene from ethane by supported liquid membranes containing silver nitrate as a carrier, J. Chem. Eng. Jpn. 19 (1986) 419–424.
[17] I. Pinnau, L.G. Toy, Solid polymer electrolyte composite membranes for olefin/paraffin separation, J. Membr. Sci. 184 (2001) 39–48.
[18] H.S. Kim, S.J. Park, D.Q. Nguyen, J.Y. Bae, H.W. Bae, H. Lee, S.D. Lee, D.K. Choi, Multi-functional zwitterionic compounds as new membrane materials for separating olefin-paraffin mixtures, Green Chem. 9 (2007) 599–604.

[19] J.C. Davis, R.J. Valus, R. Eshraghi, A.E. Velikoff, Facilitated transport membrane hybrid systems for olefin purification, Sep. Sci. Technol. 28 (1993) 463–476.
[20] O.I. Eriksen, E. Aksnes, I.M. Dahl, Facilitated transport of ethene through Nafion membranes. Part I. Water swollen membranes, J. Membr. Sci. 85 (1993) 89–97.
[21] O.I. Eriksen, E. Aksnes, I.M. Dahl, Facilitated transport of ethene through Nafion membranes. Part II. Glycerine treated, water swollen membranes, J. Membr. Sci. 85 (1993) 99–106.
[22] S.U. Hong, J.Y. Kim, Y.S. Kang, Effect of water on the facilitated transport of olefins through solid polymer electrolyte membranes, J. Membr. Sci. 181 (2001) 289–293.
[23] J. Müller, K.V. Peinemann, Development of facilitated transport membranes for the separation of olefins from gas streams, Desalination 145 (2002) 339–345.
[24] S.L. James, Metal-organic frameworks, Chem. Soc. Rev. 32 (2003) 276–288.
[25] J.R. Long, O.M. Yaghi, The pervasive chemistry of metal-organic frameworks, Chem. Soc. Rev. 38 (2009) 1213–1214.
[26] B. Chen, N.W. Ockwig, A.R. Millward, D.S. Contreras, O.M. Yaghi, High H_2 adsorption in a microporous metal-organic framework with open metal sites, Angew. Chem. Int. Ed. 44 (2005) 4745–4749.
[27] A.G. Wong-Foy, A.J. Matzger, O.M. Yaghi, Exceptional H_2 saturation uptake in microporous metal-organic frameworks, J. Am. Chem. Soc. 128 (2006) 3494–3495.
[28] H. Furukawa, O.M. Yaghi, Storage of hydrogen, methane, and carbon dioxide in highly porous covalent organic frameworks for clean energy applications, J. Am. Chem. Soc. 131 (2009) 8875–8883.
[29] S. Ma, H.C. Zhou, Gas storage in porous metal-organic frameworks for clean energy applications, Chem. Commun. 46 (2010) 44–53.
[30] S. Achmann, G. Hagen, M. Hämmerle, I. Malkowsky, C. Kiener, R. Moos, Sulfur removal from low-sulfur gasoline and diesel fuel by metal-organic frameworks, Chem. Eng. Technol. 33 (2010) 275–280.
[31] D. Zacher, O. Shekhah, C. Wöll, R.A. Fischer, Thin films of metal-organic frameworks, Chem. Soc. Rev. 38 (2009) 1418–1429.
[32] Y. Liu, Z. Ng, E.A. Khan, H.K. Jeong, C.b. Ching, Z. Lai, Synthesis of continuous MOF-5 membranes on porous α-alumina substrates, Microporous Mesoporous Mater. 118 (2009) 296–301.
[33] Y. Yoo, Z. Lai, H.K. Jeong, Fabrication of MOF-5 membranes using microwave-induced rapid seeding and solvothermal secondary growth, Microporous Mesoporous Mater. 123 (2009) 100–106.
[34] W.J. Koros, R. Mahajan, Pushing the limits on possibilities for large scale gas separation: which strategies? J. Membr. Sci. 175 (2000) 181–196.
[35] S. Basu, A. Cano-Odena, I.F.J. Vankelecom, Asymmetric Matrimid®/$[Cu_3(BTC)_2]$ mixed-matrix membranes for gas separations, J. Membr. Sci. 362 (2010) 478–487.
[36] S. Basu, A. Cano-Odena, I.F.J. Vankelecom, MOF-containing mixed-matrix membranes for CO_2/CH_4 and CO_2/N_2 binary gas mixture separations, Sep. Purif. Technol. 81 (2011) 31–40.
[37] H. Bux, C. Chmelik, R. Krishna, J. Caro, Ethene/ethane separation by the MOF membrane ZIF-8: molecular correlation of permeation, adsorption, diffusion, J. Membr. Sci. 369 (2011) 284–289.
[38] T.H. Bae, J.S. Lee, W. Qiu, W.J. Koros, C.W. Jones, S. Nair, A high-performance gas-separation membrane containing submicrometer-sized metal-organic framework crystals, Angew. Chem. Int. Ed. 49 (2010) 9863–9866.
[39] H.B. Tanh Jeazet, C. Staudt, C. Janiak, Metal-organic frameworks in mixed-matrix membranes for gas separation, Dalton Trans. 41 (2012).
[40] Y. Dai, J.R. Johnson, O. Karvan, D.S. Sholl, W.J. Koros, Ultem®/ZIF-8 mixed matrix hollow fiber membranes for CO_2/N_2 separations, J. Membr. Sci. 401–402 (2012) 76–82.
[41] C. Zhang, Y. Dai, J.R. Johnson, O. Karvan, W.J. Koros, High performance ZIF-8/6FDA-DAM mixed matrix membrane for propylene/propane separations, J. Membr. Sci. 389 (2012) 34–42.
[42] S. Kunz, O. Tangermann, M. Hartmann, C4 olefin/paraffin separation over the metal organic framework material Cu_3BTC_2, in, Hamburg, 2007, pp. 95–104.
[43] M.G. Plaza, A.F.P. Ferreira, J.C. Santos, A.M. Ribeiro, U. Müller, N. Trukhan, J.M. Loureiro, A.E. Rodrigues, Propane/propylene separation by adsorption using shaped copper trimesate MOF, Microporous Mesoporous Mater.
[44] M.G. Plaza, A.M. Ribeiro, A. Ferreira, J.C. Santos, Y.K. Hwang, Y.K. Seo, U.H. Lee, J.S. Chang, J.M. Loureiro, A.E. Rodrigues, Separation of C3/C4 hydrocarbon mixtures by adsorption using a mesoporous iron MOF: MIL-100(Fe), Microporous Mesoporous Mater. 153 (2012) 178–190.
[45] T. Visser, N. Masetto, M. Wessling, Materials dependence of mixed gas plasticization behavior in asymmetric membranes, J. Membr. Sci. 306 (2007) 16–28.
[46] T. Visser, Mixed gas plasticization phenomena in asymmetric membranes, Membr. Sci. Technol., University of Twente, Enschede, 2006, 189.
[47] T.T. Moore, R. Mahajan, D.Q. Vu, W.J. Koros, Hybrid membrane materials comprising organic polymers with rigid dispersed phases, AIChE J. 50 (2004) 311–321.
[48] T.T. Moore, W.J. Koros, Non-ideal effects in organic–inorganic materials for gas separation membranes, J. Mol. Struct. 739 (2005) 87–98.
[49] R. Sips, On the structure of a catalyst surface, J. Chem. Phys. 16 (1948) 490–495.
[50] D.D. Do, Adsorption Analysis Equilibria and Kinetics, Imperial College Press, London, 1998.
[51] J.G. Wijmans, R.W. Baker, The solution–diffusion model: a review, J. Membr. Sci. 107 (1995) 1–21.
[52] Y. Yampolskii, I. Pinnau, B.D. Freeman, Materials Science of Membranes, John Wiley & Sons Ltd., Chichester, 2007.
[53] J.N. Barsema, G.C. Kapantaidakis, N.F.A. Van Der Vegt, G.H. Koops, M. Wessling, Preparation and characterization of highly selective dense and hollow fiber asymmetric membranes based on BTDA-TDI/MDI co-polyimide, J. Membr. Sci. 216 (2003) 195–205.
[54] Sigma-Aldrich website, http://www.sigmaaldrich.com/catalog/product/aldrich/688614lang=en&region=NL.
[55] S.S.-Y. Chui, S.M.-F. Lo, J.P.H. Charmant, A.G. Orpen, I.D. Williams, A chemically functionalizable nanoporous material $[Cu_3(TMA)_2(H_2O)_3]n$, Science 283 (1999) 1148–1150.
[56] A. Einstein, Does the inertia of a body depend upon its energy-content, Annalen der. Physik. 18 (1905).
[57] S. Biswas, T. Ahnfeldt, N. Stock, New functionalized flexible Al-MIL-53-X (X=–Cl, –Br, $–CH_3$, $–NO_2$, $–(OH)_2$) solids: syntheses, characterization, sorption, and breathing behavior, Inorg. Chem. 50 (2011) 9518–9526.
[58] Z. Liang, M. Marshall, A.L. Chaffee, CO_2 adsorption-based separation by metal organic framework (Cu-BTC) versus zeolite (13X), Energy Fuels 23 (2009) 2785–2789.
[59] W.A. Herrmann, G. Brauer, Synthetic Methods of Organometallic and Inorganic Chemistry, Georg Thieme Verlag, Stuttgart, 1996.
[60] J. Xia, T.-S. Chung, P. Li, N.R. Horn, D.R. Paul, Aging and carbon dioxide plasticization of thin polyetherimide films, Polymer 53 (2012) 2099–2108.
[61] R. Mahajan, W.J. Koros, Mixed matrix membrane materials with glassy polymers, Polym. Eng. Sci. 42 (2002) 1432–1441.
[62] H.B.T. Jeazet, C. Staudt, C. Janiak, A method for increasing permeability in O_2/N_2 separation with mixed-matrix membranes made of water-stable MIL-101 and polysulfone, Chem. Commun. 48 (2012) 2140–2142.
[63] V. Stannett, The transport of gases in synthetic polymeric membranes. A historic perspective, J. Membr. Sci. 3 (1978) 97–115.
[64] D.R. Paul, Gas sorption and transport in glassy polymers, Berichte der Bunsengesellschaft für physikalische Chemie 83 (1979) 294–302.